Journal of Experimental Botany, Vol. 76, No. 22 pp. 7051–7066, 2025
https://doi.org/10.1093/jxb/eraf381 Advance Access Publication 2 September 2025

RESEARCH PAPER

Jasmonic acid signalling is targeted by a smut fungal Tin2-fold effector

Summia Gul[1], Gabriel Mendoza-Rojas[1,], Max Heinen[1], Natascha Heßler[1,], Stefanie Galle[2], Jürgen Zeier[3,], Sander H. J. Smits[2,4,], Florian Altegoer[1,*,], and Vera Göhre[1,†,*,]

[1] Institute of Microbiology, Cluster of Excellence on Plant Sciences, Heinrich-Heine University Düsseldorf, 40225 Düsseldorf, Germany
[2] Center for Structural Studies, Heinrich Heine University Düsseldorf, 40225 Düsseldorf, Germany
[3] Institute of Molecular Ecophysiology of Plants, Cluster of Excellence on Plant Sciences, Heinrich-Heine University Düsseldorf, 40225 Düsseldorf, Germany
[4] Institute of Biochemistry, Heinrich Heine University Düsseldorf, 40225 Düsseldorf, Germany

* Correspondence: Vera.Goehre@uni-duesseldorf.de or altegoer@hhu.de
† Present address: Hochschule Darmstadt, 64295 Darmstadt, Germany.

Received 9 July 2024; Accepted 29 August 2025

Editor: Monica Höfte, University of Ghent, Belgium

Abstract

Jasmonate signalling integrates environmental cues with plant growth and development. Owing to its role in balancing defence responses against pathogens, it is a target of effector proteins from various pathogens. Here, we characterized the fungal effector protein Tue1 from the Brassicaceae smut fungus *Thecaphora thlaspeos*, which naturally infects *Arabis hirsuta* but can also colonize *Arabidopsis thaliana*. *In planta*, Tue1 hijacks the plant importin-α-dependent nuclear transporter to reach the plant nucleus. We demonstrate that Tue1 interacts with jasmonate ZIM-domain 10 (JAZ10) proteins of both *A. thaliana* and *A. hirsuta*. Structure-guided analysis of Tue1 suggests that it binds the Jas motif of JAZ10, indicating a role in stabilization or binding competition with proteins such as MYC3 and COI1. This is further supported by reduced jasmonate concentrations upon *tue1* overexpression in *A. thaliana* and differential regulation of a subset of jasmonate-responsive genes during *T. thlaspeos* infection of *A. hirsuta*. Tue1 is part of the Tin2-fold effector family recently described in the corn smut *Ustilago maydis*. Our study demonstrates that this effector family is expanded across smut fungal species, although further studies are needed to reveal whether targeting JAZ repressors is a conserved mechanism or specifically acquired as an adaptation to the perennial host.

Keywords: *Arabis hirsuta*, effector protein, nuclear localization, perennial pathogen, plant–microbe interaction, *Thecaphora thlaspeos*, X-ray crystallography.

© The Author(s) 2025. Published by Oxford University Press on behalf of the Society for Experimental Biology.
This is an Open Access article distributed under the terms of the Creative Commons Attribution-NonCommercial-NoDerivs licence (https://creativecommons.org/licenses/by-nc-nd/4.0/), which permits non-commercial reproduction and distribution of the work, in any medium, provided the original work is not altered or transformed in any way, and that the work is properly cited. For commercial re-use, please contact reprints@oup.com for reprints and translation rights for reprints. All other permissions can be obtained through our RightsLink service via the Permissions link on the article page on our site–for further information please contact journals.permissions@oup.com.

Downloaded from https://academic.oup.com/jxb/article/76/22/7051/8245658 by Deutsches Elektronen Synchrotron DESY user on 15 January 2026

Introduction

During plant evolution, fungi played a critical role in shaping the development of land plants (Hoeksema *et al.*, 2018). Most vascular plants form close associations with mycorrhizal fungi, which represent a key aspect of plant terrestrialization (Puginier *et al.*, 2022). In addition to these beneficial interactions, parasitic relationships between fungi and plants have also emerged, leading to numerous fungal diseases that strongly influenced ecosystems and even contributed to the extinctions of plant and animal species (Fisher *et al.*, 2012). To establish these interactions, fungi use specialized secreted proteins known as effectors, which facilitate colonization by, for example, suppressing plant immune responses or manipulating key cellular processes in the host (Lo Presti *et al.*, 2015; Lanver *et al.*, 2017). As many of these proteins evolved in the course of a specific fungal–plant interaction, they often share little sequence homology and lack domains of known function. Although effector proteins are the primary focus of research in the field of plant pathology, biochemical studies and studies focusing on structure–function relationships are still critically lacking, and the functions of most virulence factors are still poorly understood.

A large group of fungal pathogens are smut fungi, with more than 550 known Basidiomycete species. These fungi have a narrow host range and infect important crops such as maize, wheat, rice, or barley (Zuo *et al.*, 2019), peanut (Paredes *et al.*, 2024), and potato (EFSA Panel on Plant Health (PLH) et al., 2018). Smut fungi are biotrophic pathogens that rely on the viability of their infected hosts and establish an intimate interaction with them. Whereas smut species colonizing monocot hosts are best characterized due to their agronomic impact, the dicot smut fungi, in particular those from the *Thecaphora* clade (Vánky, 2008), are understudied. For example, *Thecaphora thlaspeos* naturally occurs in >15 *Brassicaceae* host plants, including *Arabis* species (Vánky, 2008), and it can colonize the non-host model plant *Arabidopsis thaliana* (Frantzeskakis *et al.*, 2017). In recent years, *T. thlaspeos* has been established as a dicot smut model system that can also be genetically modified (Plucker *et al.*, 2021). Its genome is a typical smut genome of small size (Courville *et al.*, 2019) but the effector repertoire shows some remarkable differences concerning the core effectors of grass smut fungi (Schuster *et al.*, 2018).

Effector genes of smut fungi are often but not exclusively organized in clusters that encode small protein families (Kämper *et al.*, 2006). Some of these families have been demonstrated to contribute to virulence, whereas for others no influence on the plant colonization process was observed in laboratory infections (Kämper *et al.*, 2006; Schirawski *et al.*, 2010). The sequence variability among these effector genes is high and only a small percentage is conserved among related smut species (Laurie *et al.*, 2012). The dicot-infecting smut fungi such as *Melanopsichium pennsylvanicum* and *T. thlaspeos* share an even smaller proportion of conserved effectors with their grass-infecting relatives (Sharma *et al.*, 2014; Courville *et al.*, 2019). Despite a close relationship to *Ustilago maydis* and *T. thlaspeos* at the genomic level, (Courville *et al.*, 2019) the smut fungus *Pseudozyma flocculosa* (*Anthracocystis flocculosa*), which has so far been described as an endophyte and a biocontrol agent rather than a parasite, has even lost specific subsets of effector proteins (Lefebvre *et al.*, 2013). By contrast, core effectors have been identified that are functionally conserved among dicot and monocot smuts, such as Pep1 (Hemetsberger *et al.*, 2015; Courville *et al.*, 2019). Hence, effectors can be grouped into core effectors with shared functions among smut fungi and specific effectors used by individual or small subgroups to support infection.

Previously, we identified a subset of effector candidates unique to *T. thlaspeos*. Of those, the *Thecaphora*-unique effector 1 (Tue1) caused a strong growth defect and promoted bacterial virulence upon heterologous expression *in planta* (Courville *et al.*, 2019), and has therefore turned out to be a promising candidate for further investigation. Here, we now provide a detailed characterization of Tue1 and give insights into its molecular function in interfering with plant hormone signalling. Our structure-guided approach reveals that Tue1 belongs to an expanded family of smut fungal effectors that do not share sequence similarities but have a common structural core. While the characterization of Tue1 in the infection biology of *Brassicaceae* gives insight into how a perennial pathogen modifies the plant during the extended biotrophic phase, in the future this core structure might be used as a tool to modify plant hormone signalling.

Materials and methods

Accession numbers and sequence analysis

Arabidopsis thaliana sequences were taken from TAIR (*AtJAZ10* = At5g13220.1, *AtMYC3* = At5g46760). *Thecaphora thlaspeos* sequences for Tue1 (THTG_04687) and Tue16 (THTG_04669) and *Arabis hirsuta* sequences for JAZ10 (ArH_00064583-RA) were taken from our genome and transcriptome sequencing (Courville *et al.*, 2019). Nuclear localization sequences were predicted using NLStradamus (Nguyen Ba *et al.*, 2009), Localizer (Sperschneider *et al.*, 2017), and cNLSmapper (Kosugi *et al.*, 2009).

DNA amplification and molecular cloning

tue1 and *tue16* were amplified from cDNA of *T. thlaspeos* strain LF1, excluding the signal peptide (Courville *et al.*, 2019). *AtMYC3* (5-242) and *AtJAZ10* were amplified from cDNA of *A. thaliana* Col-0, and *AhJAZ10* was amplified from cDNA of *A. hirsuta* RH2015. Expression constructs for the effectors under the control of the 35S promoter in *Nicotiana benthamiana* and *A. thaliana* were generated by Standard GreenGate cloning (Lampropoulos *et al.*, 2013). For bimolecular fluorescence complementation (BiFC) assays, *AtMYC3*(5-242), *tue16*, *tue1*, and truncated *tue1* versions were tagged with N-terminal split mVenus, and *AtJAZ10* and *AhJAZ10* were tagged with the C-terminal split mVenus. For yeast two-hybrid (Y2H) assays, *tue1* lacking the signal peptide was inserted into

Downloaded from https://academic.oup.com/jxb/article/76/22/7051/8245658 by Deutsches Elektronen Synchrotron DESY user on 15 January 2026

pGILDA (Clontech) to generate a fusion with the *lexA* gene. Plant targets identified in the Y2H screen were cloned as translational fusions with the activation domain in pB42AD (Clontech) for verification. A standard GoldenGate cloning procedure (Zweng *et al.*, 2025) was used to generate expression constructs in the pEMGB1 backbone. *tue1*, *tue16*, and *AtJAZ10* were N-terminally tagged with hexa-histidine. The solubility tag GB1 was fused to the N-terminus of JAZ10. Plasmids and oligonucleotides used in this work are listed in Supplementary Tables S1 and S2.

Strains and growth conditions

The *Escherichia coli* strain Top10 (Thermo Fisher Scientific) was used for cloning purposes. The *E. coli* strain BL21 (DE3) (Novagen) was used to express all proteins produced in this study. The *E. coli* strains were grown at 37 °C in dYT media [tryptone 1.6% (w/v), yeast extract 1% (w/v) and NaCl 0.5% (w/v)]. *Agrobacterium tumefaciens* strain C58pMP90 (Koncz and Schell, 1986) was employed the for expression of effectors in *A. thaliana* and *N. benthamiana*. The *A. tumefaciens* strains were grown at 28 °C in dYT media containing the appropriate antibiotics (100 μg ml^{-1} spectinomycin, 10 μg ml^{-1} rifampicin, 50 μg ml^{-1} gentamycin, and 10 μg ml^{-1} tetracycline). *Saccharomyces cerevisiae* strain EGY48 (Matchmaker 3 system, Clontech) was used to perform the Y2H library screen. The *S. cerevisiae* strains were grown at 30 °C in YPDA [yeast extract 1.25% (w/v), peptone 2.5% (w/v), glucose 2% (w/v), 0.008% adenine] and SD-dropout medium [amino acid mix 0.5% (w/v), yeast nitrogen base 1.7% (w/v), glucose 2% (w/v)] with shaking at 200 rpm. All strains used are listed in Supplementary Table S3.

Transgenic *Arabidopsis thaliana* lines and transient expression in *Nicotiana benthamiana*

Transgenic *A. thaliana* Col-0 lines carrying Tue1-GFP, free GFP, and nuclear localization signal (NLS)-mCherry constructs were generated via the floral dip method (Deak *et al.*, 1986). Transgenic seeds were selected on kanamycin and verified for expression of the respective fluorescent proteins. *N. benthamiana* was infiltrated by *A. tumefaciens* for transient expression of Tue1-GFP, Tue1ΔNLS-GFP, free GFP, and NLS-mCherry. Protein localization was assessed in the stable lines or in *N. benthamiana* at 3 d post infiltration by examination with a Zeiss LSM 880 confocal microscope. All plant lines used are listed in Supplementary Table S4.

Protein production and purification

Protein purification was performed as previously described (Zweng *et al.*, 2025). Briefly, *E. coli* BL21 (DE3) strains (Novagen) containing pET22b-Tue1-His were grown to an OD_{600} of 0.6 at 30 °C and protein expression was induced by treatment with 0.5 mM IPTG at 20 °C for 20 h. The cells were disrupted with a microfluidizer (M110-L, Microfluidics). Debris-free supernatant was loaded on to Ni-NTA FF-HisTrap columns (GE Healthcare) for affinity purification via the hexa-histidine tag. The eluted protein was concentrated using Amicon Ultra-10K centrifugal filters and subjected to size-exclusion chromatography using a Superdex S200 Increase 16/600 column. The peak fractions were analysed using a standard SDS-PAGE protocol, pooled, and concentrated with Amicon Ultra-10K centrifugal filters.

Selenomethionine incorporation for anomalous diffraction

Escherichia coli BL21 (DE3) strains (Novagen) containing pET22b-Tue1-His cultures were inoculated in M9 medium (37.25 g l^{-1} Na_2HPO_4, 16.5 g l^{-1} KH_2PO_4, 2.75 g l^{-1} NaCl, 5.5 g l^{-1} NH_4Cl, pH 7.5) to an OD_{600} of 0.1, infused with sterile and freshly made SolX solution (1 g l^{-1} L-lysine, 1 g l^{-1} L-threonine, 1 g l^{-1} L-phenylalanine, 0.5 g l^{-1} L-leucine, 0.5 g l^{-1} L-isoleucine, 0.5 g l^{-1} valine, 0.25 g l^{-1} selenomethionine, 80 g l^{-1} glucose, 100 mM $MgCl_2$, 10 mM $CaCl_2$), and grown to an OD_{600} of 0.6. Protein production was induced by treatment with 1 mM IPTG for 20–22 h at 37 °C. The cells were harvested and stored at −80 °C or immediately used for protein purification.

Protein crystallization

Crystallization was performed using MRC-3, 96-well sitting drop plates, and commercial crystallization screening kits at 12 °C. A 0.1 μl volume of homogeneous protein solution was mixed with 0.1 μl of reservoir solution and equilibrated against 40 μl of the reservoir. After 1 week, initial rod-shaped crystals were found, which were further optimized by slightly varying the precipitant concentrations. Optimization was conducted in 24-well sitting drop plates at 12 °C but by mixing 1 μl protein solution with 1 μl of the reservoir solution, equilibrated against 300 μl reservoir solution. Native Tue1-6H crystallized at 12 mg ml^{-1} concentration within 2 weeks in 0.05 M NaCl, 1.2 M K/Na tartrate, 0.1 M imidazole, pH 8. Se-Met Tue1-6H crystallized at 12 mg ml^{-1} concentration within 1 month in the same condition. Before harvesting the crystals, crystal-containing drops were overlaid with 2 μl mineral oil and immediately flash-frozen in liquid nitrogen.

Data collection, processing, and structure refinement

Data were collected under cryogenic conditions at the EMBL beamline P13 (Deutsches Elektronen Synchrotron; DESY). The data were integrated and scaled using XDS and merged with XSCALE (Kabsch, 2010). The structure of Tue1 was phased by isomorphous replacement using data obtained from single-wavelength anomalous dispersion gathered by incorporating selenomethionine. The structure was manually built in COOT (Emsley and Cowtan 2004) and refined with PHENIX (Adams *et al.*, 2010). The figures were prepared with ChimeraX (Pettersen *et al.*, 2021). All residues were found within the preferred and additionally allowed regions of the Ramachandran plot. Detailed data collection and refinement statistics are listed in Supplementary Table S5.

Structural analysis and clustering

Structural similarity analysis was performed using the Foldseek webserver (https://search.foldseek.com/) with the Tue1 structure as the query, yielding 1199 structural matches. These sequences were analysed using SignalP 6.0 (Teufel *et al.*, 2022), which identified 320 putative secreted candidates. After removal of redundancy and manual domain verification, 180 high-confidence candidates were retained. The dataset was supplemented with 42 characterized Tin2-fold structures from *U. maydis* and validated predicted structures for Tue1 and Tue16, for a total of 163 structures. All-vs-all pairwise alignments were performed using TM-align, and the resulting TM-score matrix was imported into Gephi (https://gephi.org/) for network analysis. Proteins were represented as nodes with edges weighted by TM-score; edges <0.4 were excluded and self-looping was disabled. Network visualization was optimized by using Fruchterman–Reingold (area=20 000; gravity=10; speed=10) and ForceAtlas2 (scaling=75; gravity=1; edge weight influence=6; noverlap) algorithms. Outliers were manually checked and verified for structural similarity and protein prediction quality. The final resulting network contained 163 nodes, each representing a protein (Supplementary Dataset S1). Node features encode the clustering coefficient, while edge gradation reflects the TM-score.

Yeast two-hybrid assays

The *S. cerevisiae* strain EGY48 was transformed with Tue1-LexA-pGILDA (Clontech, MATCHMAKER LexA Two-Hybrid System) and tested for auto-activity. A cDNA library from stress-induced *A. thaliana* in pB42AD (Matiolli and Melotto, 2018) was co-transformed with Tue1-LexA-pGILDA for screening according to the manual (Clontech). For the

Downloaded from https://academic.oup.com/jxb/article/76/22/7051/8245658 by Deutsches Elektronen Synchrotron DESY user on 15 January 2026

library transformation, the protocol was scaled up to 2400 µl competent cells and 10 µg plasmid DNA of library was used (Matiolli and Melotto, 2018).

Plasmids from interaction candidates were extracted according to the manual (Clontech). The selected prey candidates were sequenced and identified by comparison to the *A. thaliana* genome. Full-length gene models for the candidates were obtained from TAIR, and *A. hirsuta* homologs were identified from our preliminary *A. hirsuta* sequences (Courville *et al.*, 2019). Protein extraction from yeast cells expressing Tue1, AtJAZ10, and AhJAZ10 was done according to the manual (Clontech) for western blot verification of protein enrichment.

Bimolecular fluorescence complementation

Translation fusions of the effector candidates and plant targets (*AtMYC3*, *tue16*, *tue1*, and truncated versions of *tue1* tagged with N-terminal split mVenus; *AtJAZ10* and *AhJAZ10* with C-terminal split mVenus) as well as an *NLS-mCherry* construct in *A. tumefaciens* strain C58 pMP90 pSOUP were infiltrated into *N. benthamiana* leaves. Signal reconstitution of the split fluorophore was observed by confocal microscopy at 2–3 d post infiltration on a Zeiss LSM 880 microscope. Fluorescence signals were quantified using ImageJ (http://rsb.info.nih.gov/ij) and analysed by mean fluorescence intensity and the JACoP BIOP plugin (https://github.com/BIOP/ijp-jacop-b) for the total fluorescence intensity and co-localized signal intensity with the NLS marker, respectively.

Microscale thermophoresis

Recombinant 6HN-GST-MYC3 (5-242), 6HN-GST-Tue1, and 6HN-GST-Tue16 proteins were labelled with Alexa Fluor® 488 (NHS Ester, Lumiprobe GmbH, Germany). Recombinant 6HN-JAZ10 and 6HN-JAZ10C (3.1 nM–100 µM, 16 serial dilutions) were incubated with each labelled protein at 200 nM in 0.01% Tween-20-SEC buffer. A 10 µl sample was transferred into a glass capillary (NanoTemper, Munich, Germany) and thermophoresis was detected with a NanoTemper Monolith Instrument (NT.115, Munich, Germany), performed with an excitation power of 20% for 30 s and microscale thermophoresis (MST) power of 40% at an ambient temperature of ~24 °C. Triplicates of the same dilution were measured. The results were further analysed by MO Affinity Analysis software (NanoTemper, Munich, Germany). Processed data are available in Supplementary Dataset S2.

Western blotting

Target proteins transiently expressed in *N. benthamiana* and *S. cerevisiae* were isolated as described by (Rutter and Innes, 2017). Equal amounts of total protein (1–5 µg) were separated by 12% SDS-PAGE and transferred to a PVDF membrane. The membrane was blocked with 5% dry skimmed milk in Tris-buffered saline with Tween-20 and incubated overnight at 4 °C with primary antibodies specific to the target proteins. After washing, the membrane was incubated with appropriate horseradish peroxidase-conjugated secondary antibodies at room temperature. Protein bands were visualized using enhanced chemiluminescence and imaged with the LAS ChemiDoc system.

Plant hormone quantification

The concentrations of salicylic acid (SA), salicylic acid 2-O-β-D-glucoside (SAG), salicylic acid glucose ester (SGE), and jasmonic acid (JA) were quantified using gas chromatography–mass spectrometry (GC–MS)-based analyses, as described previously (Hartmann *et al.*, 2018; Yildiz *et al.*, 2023). The metabolites were extracted from leaf material of 4-week-old Tue1-GFP, GFP, and Col-0 plants. After adding a mix of internal standards, the samples were derivatized with *N*-methyl-*N*-trimethylsilyltrifluoroacetamide and injected into an Agilent 7890A/5975C GC–MS system equipped with a Phenomenex ZB-35 (30m×0.25mm×0.25 µm) capillary column as described earlier (Hartmann *et al.*, 2018; Yildiz *et al.*, 2023), and the GC–MS data were analysed using MSD ChemStation software (Agilent Technologies). For the quantitative determination of metabolites, specific peaks from ion chromatograms of derivatized analytes and related internal standards were integrated: SA (m/z 267) related to D_4-SA (m/z 271), JA (m/z 282) related to dehydrojasmonic acid (m/z 284), and SAG (m/z 267) and SGE (m/z 193) both related to salicin (m/z 268), and experimentally determined correction factors were considered. The metabolite contents were normalized to the fresh weight of the leaf samples.

Results

Tue1 localizes to the plant nucleus

In a previous study, we showed that Tue1 strongly influences the growth of *A. thaliana* upon heterologous expression, resulting in significantly smaller rosettes (Courville *et al.*, 2019). We were therefore interested to reveal the mechanism underlying this strong phenotype. Although Tue1 does not contain any predicted functional domains (Courville *et al.*, 2019), Localizer (Sperschneider *et al.*, 2017) and cNLSmapper (Kosugi *et al.*, 2009) suggested the presence of an NLS between amino acids 80 and 90 in addition to the predicted signal peptide at the N-terminus (Fig. 1A). To confirm the predicted nuclear localization, we performed heterologous expression *in planta* using GFP fusions lacking the N-terminal signal peptide in comparison to NLS-mCherry (NLS of At4g19150/N7; Cutler *et al.*, 2000). Transient expression in *N. benthamiana* showed clear nuclear localization of Tue1 (Fig. 1B). To further validate that the predicted NLS confers the nuclear localization, we generated a construct of Tue1 lacking the NLS (GGVAKRPRIS). This deletion resulted in cytoplasmic localization of the protein (Fig. 1C), suggesting that Tue1 is indeed targeted to the nucleus via this identified sequence. Tue1-GFP and its truncated variant were expressed *in planta* as full-length proteins with no visible degradation (Fig. 1D). To investigate whether this fungal NLS can be recognized by the plant nuclear import machinery, we predicted the structure of *A. thaliana* importin-α in complex with the NLS of Tue1. Our structural model is in full agreement with previous experimental importin-α structures, supporting that Tue1 is actually imported into the nucleus via a direct interaction with importin-α (Supplementary Fig. S1).

Importantly, stable overexpression of Tue1-GFP in *A. thaliana* caused strong retardation of plant growth and delayed flowering, similar to untagged Tue1 (Courville *et al.*, 2019), indicating that the fusion protein is functional (Fig. 1E, F). Similar to *N. benthamiana*, Tue1-GFP also showed clear nuclear localization in *A. thaliana* (Fig. 1G). In conclusion, we showed that Tue1 localizes to the plant nucleus via an internal NLS sequence.

The crystal structure of Tue1 reveals an α-β-α-like sandwich architecture

Sequence comparison did not give an indication towards the molecular function of Tue1; therefore, we turned to structural

Downloaded from https://academic.oup.com/jxb/article/76/22/7051/8245658 by Deutsches Elektronen Synchrotron DESY user on 15 January 2026

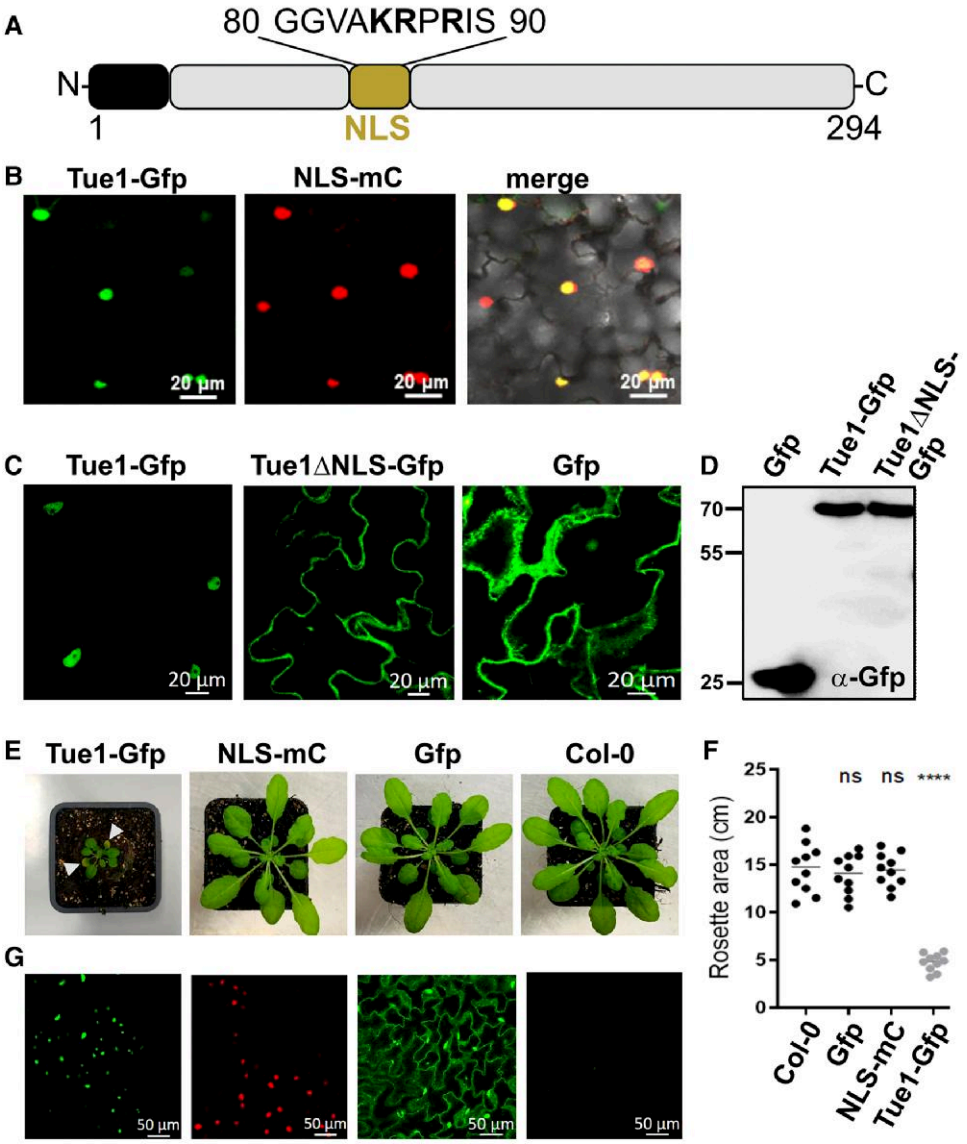


Fig. 1. Tue1 localizes to the nucleus of *Arabidopsis thaliana* and *Nicotiana benthamiana*. (A) Domain architecture of Tue1. The N-terminal signal peptide and the nuclear localization signal (NLS) are indicated. (B) Transient expression of Tue1-GFP in *N. benthamiana* at 3 d post infiltration. The left panel shows the subcellular localization of Tue1 in the nucleus. The middle panel shows the location of the nucleus, visualized by an NLS (At4g19150/N7) marker fused to mCherry (mC). The right panel shows an overlay of the GFP and mCherry channels. Yellow spots indicate co-localization of Tue1-GFP and the NLS marker in the nucleus. (C) Nuclear localization of Tue1-GFP in *N. benthamiana* in the presence and absence of the predicted NLS. The left panel indicates the fluorescence signal of Tue1-GFP, the middle panel shows the signal of Tue1ΔNLS-GFP and the right panel shows free GFP as a control. Truncation of the NLS in Tue1 leads to cytosolic localization. (D) Western blot of Tue1-GFP and Tue1ΔNLS-GFP reveals the presence of the full-length fusion proteins. (E) Macroscopic images of *A. thaliana* lines used in the microscopy experiments. The expression of Tue1-GFP resulted in chlorosis (white arrowheads) and the formation of smaller rosettes as well as delayed flowering. (F) Quantification of rosette size from the different *A. thaliana* lines, showing a significant (P<0.001) decrease in rosette size in the Tue1-GFP line. Statistical analysis was done by one-way ANOVA (with Bonferroni post-hoc test). (G) Subcellular localization of Tue1-GFP in transgenic *A. thaliana* lines. Microscopic analysis of the stable lines confirmed the nuclear localization of Tue1-GFP. NLS-mCherry clearly localizes in nuclei, whereas free GFP localizes in both the cytosol and the nuclei due to its small size. Bars=50 µm.

analysis. Unfortunately, prediction tools such as AlphaFold2 (Jumper *et al.*, 2021) failed to yield reliable results. Therefore, we crystallized the protein to obtain structural insights. Tue1 consists of 294 amino acids with a predicted molecular weight of 32.6 kDa. We produced Tue1 lacking its signal peptide in *E. coli* and purified the protein using a two-step purification protocol (Zweng *et al.*, 2025) (Supplementary Fig. S2). We determined the crystal structure of Tue1 at 1.3 Å resolution, using selenomethionine single-wavelength anomalous dispersion (Supplementary Table S5), as models obtained by using AlphaFold2 (Jumper *et al.*, 2021) were not of suitable quality for structure solution by molecular replacement. Amino acids

Downloaded from https://academic.oup.com/jxb/article/76/22/7051/8245658 by Deutsches Elektronen Synchrotron DESY user on 15 January 2026

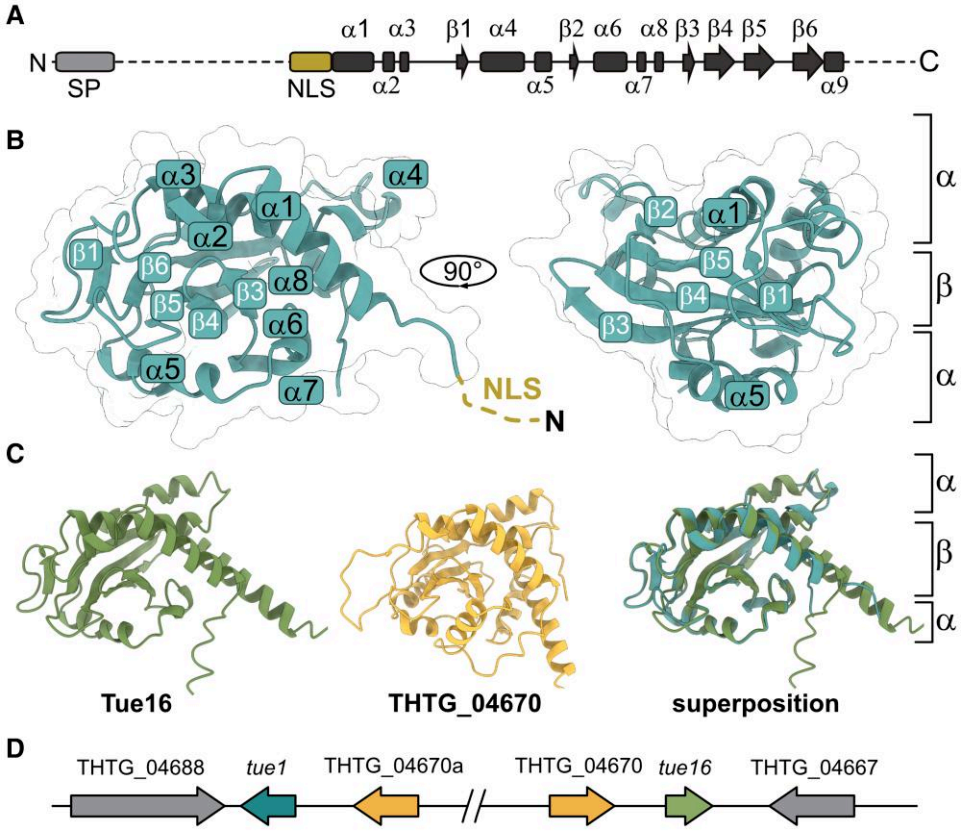


Fig. 2. Crystal structure of Tue1. (A) Domain architecture and secondary structure elements of Tue1. The signal peptide (SP) and nuclear localization sequence (NLS) are highlighted. Regions not resolved in the electron density are indicated with dashed lines. (B) Crystal structure of Tue1 displayed as a cartoon. The position of the NLS is directly adjacent to α-helix α1 and is displayed as a dashed line. The overall fold resembles an α-β-α sandwich. (C) Superposition of the predicted structures of Tue1 (teal), Tue16 (green), and THTG_04670 (orange). (D) Genomic region containing *tue1*, *tue16*, and THTG_04670, with the different genes coloured according to the predicted structures.

86 to 257 could be unambiguously modelled into the electron density, revealing eight α-helices and six β-strands that fold into a α-β-α like sandwich structure (Fig. 2A, B). The first four α-helices form the upper part of the structure, which is separated from α-helices 5–8 by a six-stranded β-sheet (Fig. 2B). The predicted NLS of Tue1 is directly adjacent to helix α1 but could not be resolved in our structure, likely due to flexibility. This supports that the cytosolic localization of the NLS deletion construct (Fig. 1D) is not caused by altered protein structure, but is due to lack of interaction with the nuclear import machinery (Supplementary Fig. S1).

Interestingly, *tue16*, a second *T. thlaspeos* effector-encoding gene, is located on contig 31 in the vicinity of *tue1*, and the proteins have a sequence identity of 68.7% (Supplementary Fig. S3). To compare the two related effector candidates, we predicted the structural model of Tue16 using AlphaFold2 through ColabFold. As expected, Tue16 is structurally highly similar to Tue1, with a root mean square deviation (RMSD) of 0.62 (132 Cα) (Fig. 2C). As observed before for Tue1, the prediction quality of the structure of Tue16 was low due to the lack of available similar sequences in the UniRef database until we used the X-ray structure of Tue1 as query. When inspecting the genomic context, we observed that the whole locus was apparently duplicated, with *tue1* and *tue16* diverging on the sequence level, whereas the two copies of another gene, *THTG_04670*, retained a nucleotide sequence identity of 99.8% in a 3 kb region of the genomic locus (Fig. 2D; Supplementary Fig. S3). We therefore also predicted the structural model of THTG_04670, which has an RMSD to Tue1 of 2.2 (104 Cα) (Fig. 2C). Both Tue16 and THTG_04670 share the general architecture of several α-helices surrounding a central β-sheet, with the surrounding α-helices being slightly displaced in THTG_04670. In contrast to Tue1 and Tue16, THTG_04670 does not contain a predicted signal peptide (Supplementary Fig. S3) and also shows deviation in the region of the potential NLS. It will be interesting to study whether THTG_04670 also has virulence activity. In conclusion, determination of the crystal structure of Tue1 revealed an α-β-α-like sandwich structure that is also shared with another potential effector, Tue16, and another protein of as yet unknown function, THTG_04670.

Downloaded from https://academic.oup.com/jxb/article/76/22/7051/8245658 by Deutsches Elektronen Synchrotron DESY user on 15 January 2026

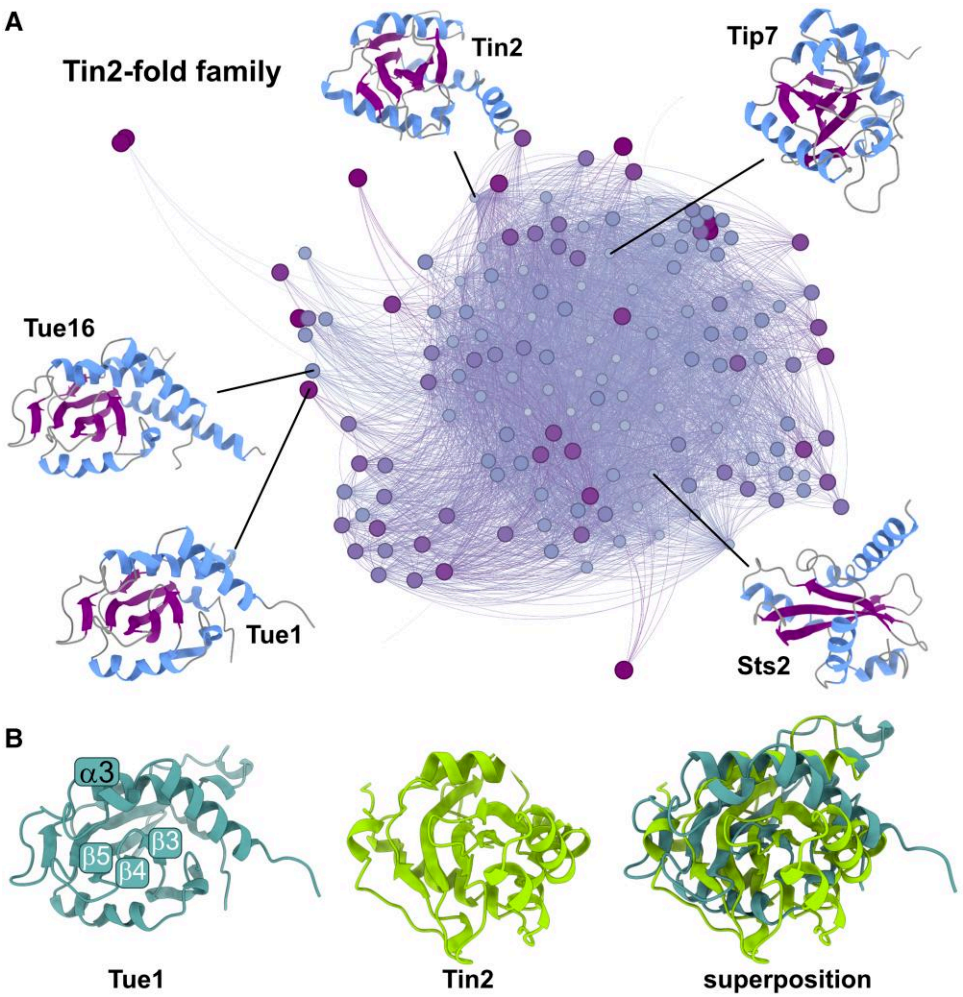


Fig. 3. Tue1 belongs to the Tin2-fold family that is expanded in smut fungi. (A) A structural clustering network of 163 Tue1-related Tin2-fold candidates in smut fungi reveals a broad structural conservation. The network visualization depicts structural relationships among proteins, with nodes representing individual structures and edges indicating structural similarity. Node characteristics (size and colour intensity) reflect local clustering coefficients, with larger, darker nodes indicating greater structural similarity with their direct neighbours. Edge colouring corresponds to TM-score; darker edges indicate higher values. Models of Tue1, Tue16 and the three characterized examples Tin2, Tip7, and Sts2 are shown. (B) Structural comparison of Tue1 and Tin2.

Tue1 is part of an extended structural effector protein family of smut fungi and shares structural homology with intracellular effector proteins of *Ustilago maydis*

With the structural information at hand, we asked whether we could identify structural homologs of Tue1 in other plant pathogens. A structural conservation of this fold would potentially enable conclusions to be drawn about the possible function of Tue1 during plant infection. We therefore performed a structural BLAST search using FoldSeek (van Kempen *et al.*, 2023) with the crystal structure of Tue1 as query.

We restricted our search to the group of the Ustilaginales as previous searches did not result in significant hits with a convincing structural homology in other organisms. After curation, we identified 224 structural homologs of Tue1 from different smut fungal species, with global TM-scores ranging from 0.9 to 0.4 (Fig. 3A; Supplementary Dataset S1). Identified candidates were compared with each other using TM-align (Zhang and Skolnick, 2005), resulting in a structural network (Fig. 3A). Notably, we identified many effector proteins from the well-characterized smut fungus *U. maydis* that were previously grouped into a structural family termed the Tin2-fold (Seong and Krasileva, 2023). Overall, we now identified structural homologs of this Tin2-fold across smut fungal species. Mostly, these proteins shared less than 15% sequence identity and the majority was still uncharacterized. We therefore looked more closely at the candidates from *U. maydis* with the highest structural similarities. Notably, Tin2 (A0A0D1BW91), Sts2 (A0A0D1BWA6), and Tip7 (A0A0D1DUN4) showed an overall similar structural architecture to Tue1 (Fig. 3A). Tin2 has been thoroughly characterized and acts on the maize protein kinase ZmTTK1, thereby

Downloaded from https://academic.oup.com/jxb/article/76/22/7051/8245658 by Deutsches Elektronen Synchrotron DESY user on 15 January 2026

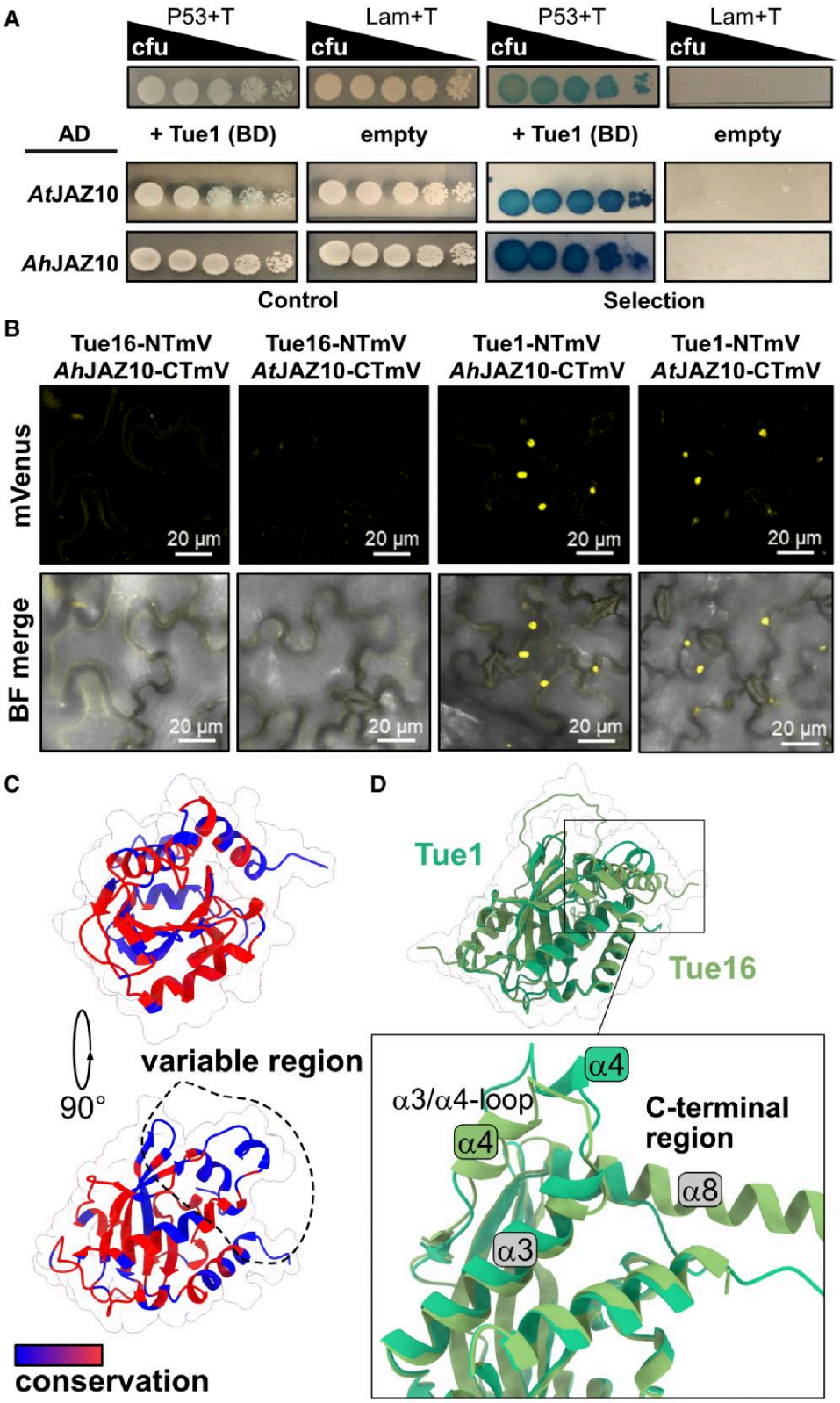


Fig. 4. JAZ10 homologs from *Arabidopsis thaliana* and *Arabis hirsuta* bind Tue1 but not Tue16. (A) Targeted yeast two-hybrid (Y2H) assay showing *in vivo* interaction of both JAZ10 homologs with Tue1. A stringent variant of the Y2H assay with X-Gal overlay for expression of a second reporter (*LacZ* gene) shows comparable results by the accumulation of a blue colour with different intensities. Lam (BD)+SV40 T-antigen (AD) as a negative control and P53 (BD)+SV40

Downloaded from https://academic.oup.com/jxb/article/76/22/7051/8245658 by Deutsches Elektronen Synchrotron DESY user on 15 January 2026

Fig. 4. Continued.
T-antigen (AD) as a positive control are shown at the top of each panel. Triple dropout medium (SD-His-Trp-Ura) was used for the control and quadruple dropout medium (SD-His-Trp-Ura-Leu) was used for the selection. (B) Interaction *in planta* was shown by bimolecular fluorescence complementation (BiFC). mVenus (mV) split parts were reconstituted and accumulated fluorescence signal in the nucleus upon interaction of the fused proteins. Tue16 did not show any fluorescence signal. Fluorophore reconstitution was also detected for the positive control MYC3. BF, bright field. Bars=20μm. (C) Based on sequence alignment, Tue1 has a variable region comprising the α4/α5-loop (residues 147–160) and the C-terminal region including α9 (250–257). (D) The variable region of Tue1 shows a slight structural variance compared with Tue16, which might explain the differences in binding to JAZ10. The inset shows a close-up of the structural regions with the greatest differences, with secondary structure elements labelled accordingly.

inducing anthocyanin biosynthesis during plant colonization by *U. maydis* (Tanaka *et al.*, 2014). It is an intracellular effector protein but it does not localize to the nucleus. A closer inspection of the structural elements of Tue1 and Tin2 revealed that the two proteins also show structural differences (Fig. 3B). The central β-sheet and spatial positioning of helices α3 and α5 are similar in both proteins, but structural elements decorating the central fold show differences (Fig. 3B). Despite Tue1 and Tin2 belonging to the same structural effector family, these structural deviations therefore suggest functional diversification by adapting the core structure. This observation was further supported by the rather remote location of Tue1 and Tue16 in our structural comparison network (Fig. 3A). Although they share the overall similar Tin2-fold, other members of this group are more closely related to each other, and the chosen *U. maydis* candidates have more central positions in the Tin2-fold family network (Fig. 3A).

In conclusion, our structural analysis of Tue1 revealed that this protein is not unique to *T. thlaspeos* as anticipated from the primary sequence but is a member of the Tin2-fold family, a structural effector family previously reported in *U. maydis* (Seong and Krasileva, 2023) and expanded in smut fungi.

Tue1 interacts with the jasmonate-ZIM domain protein JAZ10

Functional diversification based on a structural scaffold is a common principle that enables pathogens to evolve target binding while maintaining a robust core scaffold (Derbyshire and Raffaele, 2023). As the structure of Tue1 did not show similarities to enzymes or nucleic acid-binding proteins, we followed up the hypothesis that Tue1 might target host proteins in the plant nucleus. We therefore aimed to identify potential plant targets in a Y2H analysis. We used a stress-induced cDNA library of *A. thaliana* leaves that were exposed to various biotic and abiotic stresses, such as chemical treatments and bacterial inoculation (Matiolli and Melotto, 2018). Tue1 lacking the signal peptide was used as a bait. Co-transformation of a Tue1 expression plasmid with the prey pB42AD plasmid revealed no auto-activation upon analysis of the reporter gene (Supplementary Fig. S4A). This confirms that Tue1 does not possess any elements that might facilitate direct transcriptional regulation as has been described, for example, for the activation domain in the b transcription factors TtbW1 and TtbW2 (Frantzeskakis *et al.*, 2017). Expression of the full-length Tue1-LexA-DNA binding domain (DBD) was confirmed by western blotting (Supplementary Fig. S4B).

In total, we identified 140 potential interaction partner candidates in the screen, for which the respective plasmids were individually transformed to exclude auto-activation and co-transformed with the Tue1 bait vector for validation. Sequencing confirmed in-frame fusions with the DBD and narrowed the candidate list down to 129 candidates and 110 unique genes (Supplementary Dataset S3). Many of the encoded proteins show functions related to photosynthesis, for example, subunits of the photosystems or Rubisco. Since Tue1 is localized in the nucleus, we filtered the candidates accordingly. Using SUBA5 (Hooper *et al.*, 2017), we limited our list to 13 candidates with nuclear localization (Supplementary Table S6). Among these, JAZ10 attracted our attention, as we previously noticed that plant hormone-regulated genes are differentially expressed during infection (Courville *et al.*, 2019) and JAZ proteins are known targets of several effector proteins interfering with plant defence hormone signalling (Tanaka *et al.*, 2015). We therefore focused on this candidate to validate and characterize the interaction in more detail.

Tue1 but not Tue16 interacts with JAZ10 proteins from *Arabis hirsuta* and *Arabidopsis thaliana*

To confirm the interaction of Tue1 with JAZ10 using full-length proteins, we cloned the gene encoding JAZ10 from *A. thaliana* and identified the homologs from the natural host *A. hirsuta* in our transcriptome dataset (Courville *et al.*, 2019). AhJAZ10 has an amino acid sequence identity of 83% with AtJAZ10 and contains the conserved CMID, ZIM, and Jas motifs (Supplementary Fig. S5A). A targeted Y2H assay with Tue1 and both JAZ10 proteins from *A. thaliana* and *A. hirsuta* (Supplementary Fig. S5B) confirmed that the JAZ10 proteins from both plants interact with Tue1 (Fig. 4A). In a next step, we aimed to confirm the interaction by BiFC in *N. benthamiana*. Tue1 was fused to the N-terminal half of mVenus and the two JAZ10 proteins were fused to the C-terminal half of mVenus. We used Tue16 as control, as we previously showed that Tue1 and Tue16 have high structural similarity and share the NLS sequence, but show differences at the sequence level (Fig. 2C). As positive control, we used a truncated version of the transcription factor MYC3 from *A. thaliana*, a known target of the JAZ10 repressor protein

Downloaded from https://academic.oup.com/jxb/article/76/22/7051/8245658 by Deutsches Elektronen Synchrotron DESY user on 15 January 2026

(Fernández-Calvo et al., 2011) that contained only the Jas-binding domain.

The co-transformation of MYC3 and Tue1 with both JAZ10 homologs showed a clear mVenus fluorescence in the nucleus, whereas we did not observe any fluorescence when using Tue16 (Fig. 4B). Therefore, our BiFC experiments confirmed the interaction between Tue1 and JAZ10, whereas the closely related paralog Tue16 does not interact with JAZ10 and potentially targets different interaction partners. To investigate the differences between Tue1 and Tue16 that might hint at changes in target specificity or even provide insights about the possible JAZ10 binding site of Tue1, we compared the two structures in more detail. As outlined earlier, the structures of Tue1 and Tue16 are overall highly similar (Fig. 2C). Colouring the structure of Tue1 based on the sequence alignment, one region comprising the α3/α4-loop (residues 147–160) and the C-terminal region including α8 (250–257) show a larger degree of sequence variability (Supplementary Fig. S3; Fig. 4C). These regions also show a slight structural difference (Fig. 4D). Although we cannot rule out that this is a result of the lower confidence of the Tue16 prediction in this region, it might hint to a possible binding interface with JAZ10.

Next, we aimed to validate the Tue1–JAZ10 interaction *in vitro*. Tue1, Tue16, and AtJAZ10 were heterologously produced in *E. coli*. We furthermore produced the Jas-binding domain of MYC3 from *A. thaliana,* which was previously used as a positive control in our BiFC experiments (MYC3 5-242). Tue1, Tue16, and MYC3 were fluorescently labelled and subjected to MST (Supplementary Dataset S2). AtJAZ10 was titrated in decreasing concentrations starting from 100 μM. We determined a K_d of 0.43±0.38 μM for the MYC3–JAZ10 interaction, which is in line with the K_d of 0.47 μM determined previously for the JAZ10^{CMID}–MYC3 interaction (Takaoka *et al.*, 2022). The K_d of the interaction between Tue1 and JAZ10 was substantially lower at 72.53±0.94 μM (Supplementary Fig. S6A; Supplementary Table S7). In accordance with our BiFC experiments, no interaction of Tue16 and JAZ10 could be observed (Supplementary Fig. S6A). To further dissect the binding interface, we employed a JAZ10-CT construct lacking the N-terminal CMID domain. With this truncated version, Tue1 showed a significantly increased affinity of 30.98±0.57 μM, while MYC3 binding was strongly reduced (K_d=90.55±0.64 μM), indicating that Tue1 preferentially interacts with the Jas domain (Supplementary Fig. S6B). Our MST experiments therefore confirm the direct interaction between Tue1 and JAZ10, and further show that Tue16, despite being closely related to Tue1, is not capable of interacting with JAZ10. These findings furthermore suggest that Tue1 does not compete with MYC3 for CMID binding but may compete for access to the Jas domain.

JAZ10 interacts with the C-terminal region of Tue1

Unfortunately, several attempts to reconstitute the Tue1–JAZ10 complex for structural analysis were unsuccessful, and the low confidence of our structural models also prevented complex prediction through AlphaFold2. We therefore decided to follow a structure-guided approach to identify the JAZ10-binding interface of Tue1. Two truncation constructs of *tue1* were generated that code for versions of the protein either lacking the N-terminal residues 24 to 79 (Fig. 5A, Tue1-ΔN) or the C-terminal residues 274 to 294 (Fig. 5A, Tue1-ΔC). Again, we used a targeted Y2H assay with Tue1, Tue1-ΔN, and Tue1-ΔC and with JAZ10 from *A. thaliana* (Fig. 5B). The Y2H assay confirmed the interaction of all Tue1 constructs with AtJAZ10 but did not show strong differences between full-length Tue1 and the truncated versions.

We therefore employed a more sensitive assay and fused Tue1 to the N-terminal half of mVenus for transient expression in *N. benthamiana*. AtJAZ10 fused with the C-terminal split mVenus was co-transformed with full-length Tue1 and its truncated versions. Notably, the Tue1 truncations still contained the NLS necessary for nuclear localization and the structural core of the protein containing the Tin2-fold domain (Fig. 5A). MYC3 and Tue16 were used as controls. We furthermore included an NLS-mCherry construct in our experiment, which allowed us to evaluate not only nuclear co-localization, but also fluorescence signal correlation and quantification. We observed nuclear localization for MYC3, Tue1, and the two truncated Tue1 versions, which also correlated with NLS-mCherry fluorescence, indicating that JAZ10 is able to bind to all versions of the protein (Fig. 5C). However, we observed a slightly lower fluorescence intensity of co-expressed Tue1ΔC and AtJAZ10 (Fig. 5C). We therefore quantified the fluorescence signal intensity for both mCherry and mVenus through mean fluorescence intensity and Pearson's coefficient. This analysis unambiguously revealed that the fluorescence intensity of Tue1, Tue1ΔN, and MYC3 co-expressed with AtJAZ10 correlated with mCherry fluorescence, whereas the signal intensity of Tue1ΔC in combination with JAZ10 decreased significantly (Fig. 5D, E) to almost 50%. The C-terminal residues 274 to 294 also contain helix α8, which is absent in Tue16 (Fig. 5E), supporting that JAZ10 is indeed binding to that region of Tue1. To rule out that this observation is a result of lower protein expression of Tue1ΔC, we performed western blotting (Supplementary Fig. S7) This confirmed that Tue1ΔC fused to the N-terminal half of mVenus is expressed *in planta* in a comparable amount as the full-length Tue1 fusion construct (Supplementary Fig. S7). In conclusion, our structure-guided BiFC experiments revealed that JAZ10 likely binds to an interface on Tue1 that involves the C-terminal residues of Tue1, and the lack of the C-terminal region destabilized the interaction significantly.

Overexpression of Tue1 affects phytohormone accumulation in *Arabidopsis thaliana*

To test the effect of Tue1 on plant gene expression, we had previously generated *A. thaliana* lines overexpressing *tue1* and compared the SA-dependent defence gene expression of these

Downloaded from https://academic.oup.com/jxb/article/76/22/7051/8245658 by Deutsches Elektronen Synchrotron DESY user on 15 January 2026

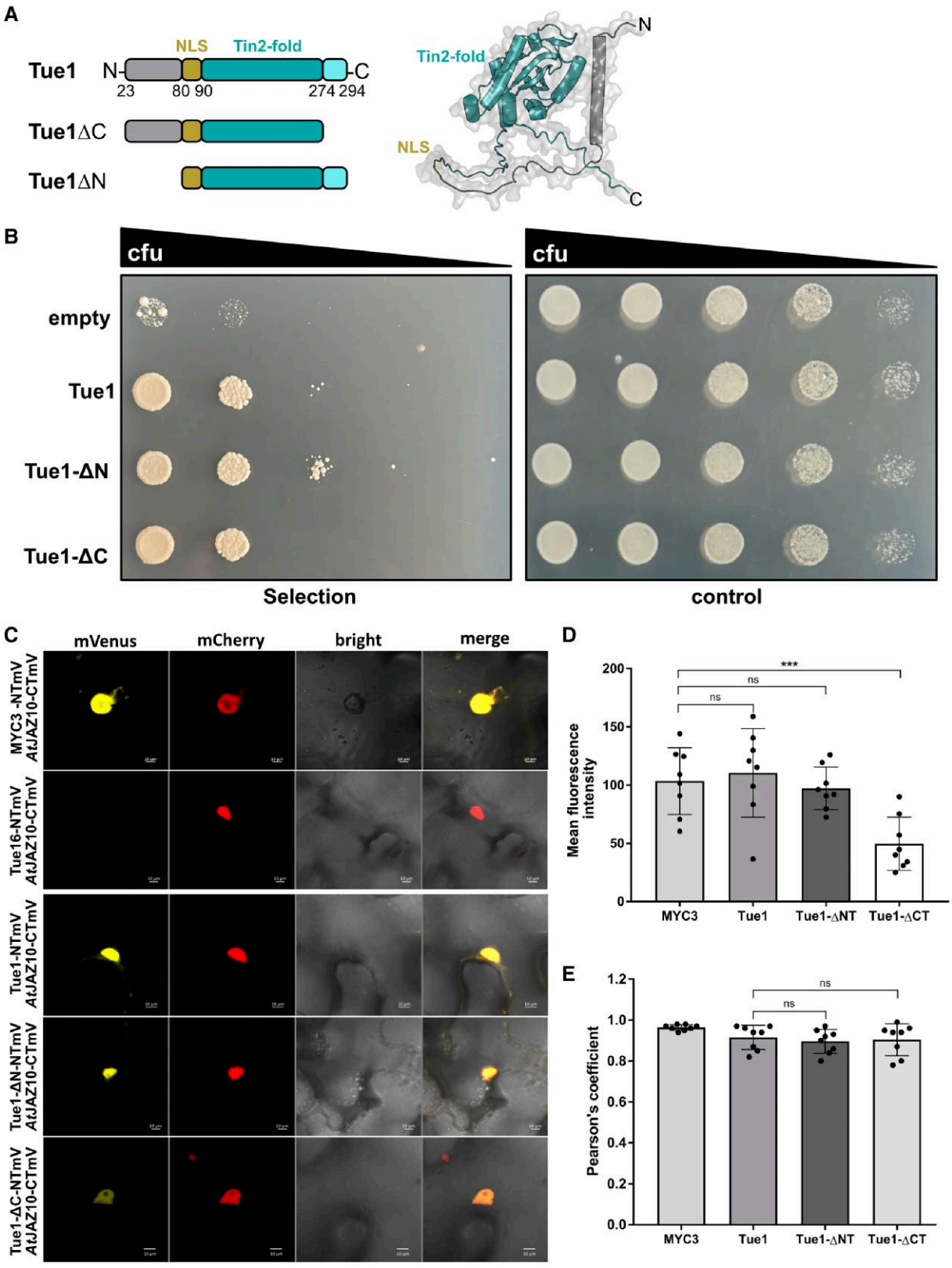


Fig. 5. JAZ10 binds to a Tue1 interface that involves the C-terminal residues. (A) Two truncated constructs of Tue1 were generated that lacked either the N-terminal residues 1–79 (Tue1-ΔN) or the C-terminal residues 274–294 (Tue1-ΔC). Both truncations still contain the NLS sequence necessary for nuclear

Downloaded from https://academic.oup.com/jxb/article/76/22/7051/8245658 by Deutsches Elektronen Synchrotron DESY user on 15 January 2026

Fig. 5. Continued.
localization and the structural core of the protein containing the Tin2-fold domain. (B) Targeted Y2H assay showing *in vivo* interaction of the truncated Tue1 versions with AtJAZ10. Triple dropout medium (SD-His-Trp-Ura) was used for the control and quadruple dropout medium (SD-His-Trp-Ura-Leu) was used for the selection. (C) The constructs fused with the N-terminal half of mVenus (Tue1-NTmV, Tue1-ΔN-NTmV, Tue1-ΔC-NTmV, MYC3-NTmV) were co-expressed with the JAZ10-CTmV in *Nicotiana benthamiana*. NLS-mCherry was co-expressed as a nuclear marker. (D, E) Quantification of the fluorescence intensity of mCherry and mVenus by measuring the mean fluorescence intensity (D) and Pearson's coefficient (E). The fluorescence intensity of Tue1, Tue1-ΔN, and MYC3 correlated with mCherry, whereas the signal intensity was significantly reduced to 50% in Tue1-ΔC. Bars indicate the mean ±SE for n=10 technical replicates. Asterisks indicate significant differences (***P<0.05; ns, not significant; unpaired, two-tailed t-test).

lines to that during natural *T. thlaspeos* infection in *A. hirsuta*. Several SA-responsive marker genes, such as *PR-1* (67-fold in *tue1*-overexpressing lines; 4.5-fold during *A. hirsuta* infection), were clearly induced (Courville *et al.*, 2019). To now address whether the presence of Tue1 directly affects phytohormone levels, we measured the concentrations of SA and JA in leaves of these plants. JA is found at low concentrations in wild-type (Col-0) and transgenic GFP-expressing lines, and it drops below the detection limit in *tue1*-overexpressing lines. By contrast, the concentrations of salicylates, namely SA, SGE, and SAG, are strongly increased when Tue1 is overexpressed compared with the control lines (Fig. 6A). This finding suggests that Tue1 interferes with the hormone crosstalk between SA and JA, likely via binding to JAZ10. We consider it likely that Tue1 stabilizes JAZ10, preventing its degradation, since SA concentrations are strongly increased and JA concentrations are reduced.

Discussion

Tue1 was previously identified as one of the *Thecaphora*-unique effector candidates that strongly impacted plant development upon overexpression in *A. thaliana* (Courville *et al.*, 2019). Here, we performed a detailed analysis of this effector protein, providing insights into its molecular function. *In planta*, Tue1 interacts with JAZ10, a repressor of jasmonate signalling. Our structural analysis furthermore revealed that Tue1 is a member of the Tin2-fold family, a previously identified structural family of effector proteins in *U. maydis* (Seong and Krasileva, 2023) with at least two members in the *T. thlaspeos* genome. Notably, there is also structural similarity to effectors from other smut fungi, which is not reflected at the sequence level.

Structural similarity but functional diversity among Tin2-fold smut fungal effectors

Recent advancements in computational methodologies for protein structure prediction, such as AlphaFold (Jumper *et al.*, 2021) and RosettaFold (Mansoor *et al.*, 2023; Krishna *et al.*, 2024), have enabled genome-wide structural predictions of effector proteins. These approaches have unveiled that certain effectors, despite being unrelated at the sequence level, form structural classes that are often distributed across a variety of host–pathogen systems, examples being RNAse-fold or ToxA-like effectors (Derbyshire and Raffaele, 2023; Seong and Krasileva, 2023). Members of these families were known previously but their broad distribution across different pathogens was an astonishing new finding.

Here, we show that the previously reported Tin2-fold family is not exclusive to *U. maydis* but can also be found in the distantly related smut *T. thlaspeos*, with Tue1 and Tue16 sharing the structural core fold (Fig. 2B, C). Based on these initial findings, we searched for structural homologs of Tue1 across smut fungi, revealing a broad distribution of the Tin2-fold family (Fig. 3A). In *U. maydis*, the majority of these genes are located within gene cluster 19A, a 40 kb genomic segment that is crucial for virulence (Kämper *et al.*, 2006; Brefort *et al.*, 2014). The effector Tin2 (UMAG_05302), also encoded within this segment, promotes virulence by sequestering maize protein kinases, thereby altering anthocyanin biosynthesis (Tanaka *et al.*, 2014; Tanaka *et al.*, 2019). Another effector that shares the Tin2-fold, Sts2 (previously Tin4; UMAG_05318) (Fig. 3A) that is also located within cluster 19A, has recently been shown to interact with plant NECAP1, acting as a transcriptional activator to regulate tumour formation (Zuo *et al.*, 2023). Further examples are effectors from the Topless interacting (Tip) family that also have a Tin2-like fold (Fig. 3A) and bind to maize TPL proteins to modify the transcriptional regulation of the host (Huang *et al.*, 2024; Khan *et al.*, 2024).

Interestingly, cluster 19A is heavily rearranged in *T. thlaspeos*, with all Tin2-fold effector encoding genes being lost from this genomic region (Courville *et al.*, 2019). However, our structural analysis now demonstrates that *T. thlaspeos* has not lost all Tin2-fold effectors, as Tue1 and Tue16, which are both encoded in a small gene cluster, belong to this structural family. Interestingly, Tue16 shares a high sequence identity of 68.8% with Tue1 and is likely also translocated into the plant nucleus due to a conserved NLS, but it does not bind to JAZ10. This observation is supported by a previous study on Tin2 showing that sequence-related Tin2 homologs from the head smut fungus *Sporisorium reilianum* have functionally diverged from their *U. maydis* counterpart (Tanaka *et al.*, 2019).

Overall, our structural analysis suggests that the Tin2-fold family is shared among all smut fungi for which genomic information is available (Fig. 3A). These effectors bind a variety of host targets and, although some share common targets (e.g. Tip6 and Tip7), they seem not to be functionally redundant (Khan *et al.*, 2024). As suggested earlier for other structural classes of effectors (Derbyshire and Raffaele, 2023), the Tin2-fold might have evolved early on in smut fungi and serves as a robust scaffold to mediate different protein–protein

Downloaded from https://academic.oup.com/jxb/article/76/22/7051/8245658 by Deutsches Elektronen Synchrotron DESY user on 15 January 2026

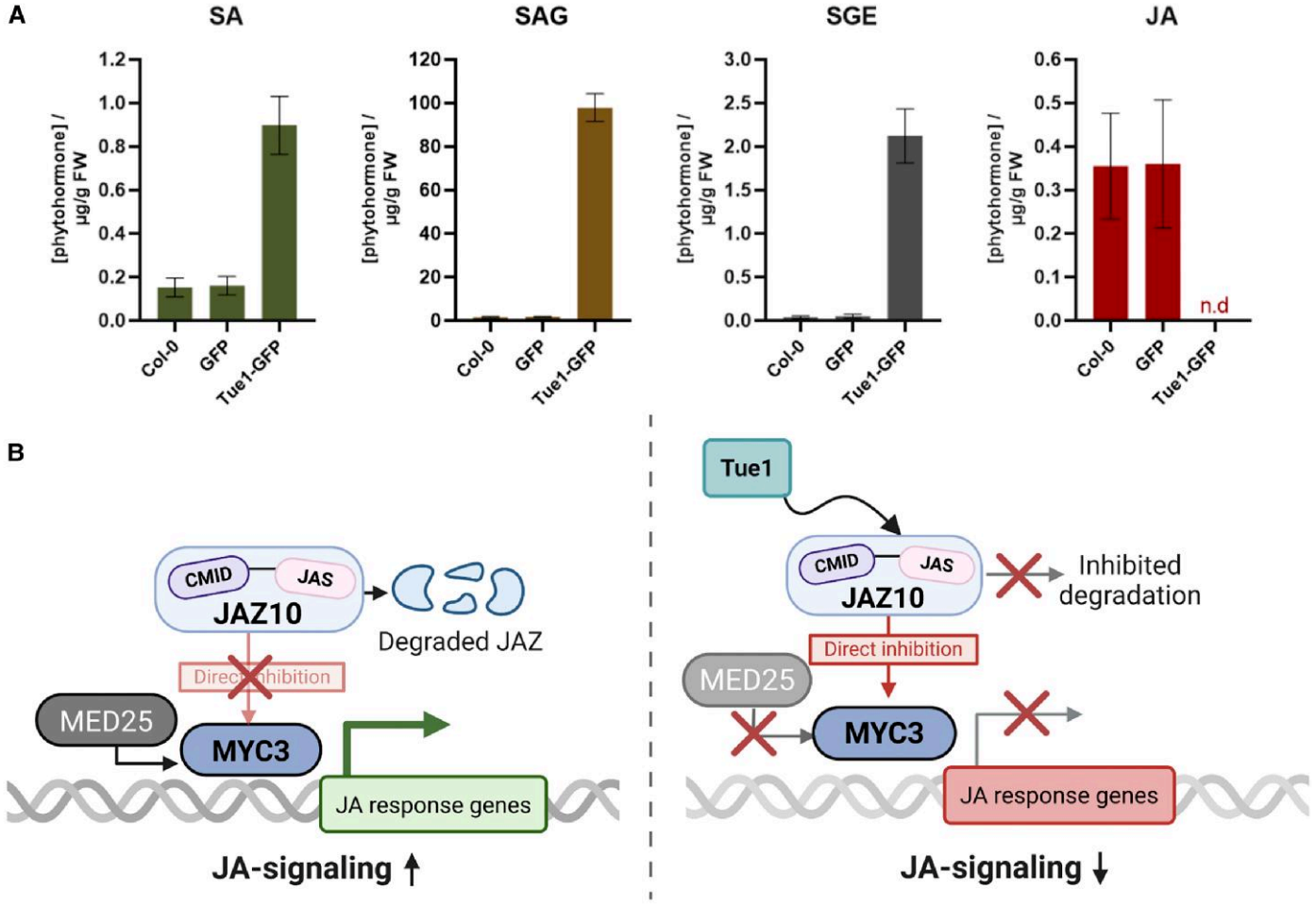


Fig. 6. Schematic overview of the possible function of Tue1 during plant colonization. (A) Overexpression of Tue1 modulates phytohormone concentrations in *Arabidopsis thaliana*. Leaf samples from 4-week-old plants were used for vapour-phase extraction, and the accumulation of metabolites was analysed by GC–MS. The Tue1-GFP line exhibited elevated concentrations of salicylic acid (SA) and its derivatives salicylic acid glucoside (SAG) and salicylic acid glucose ester (SGE), compared with the control lines (Col-0 and Col-0-GFP). In contrast, jasmonic acid (JA) concentrations were significantly reduced in the Tue1-GFP line compared with the control lines. Mean values were calculated from four biological replicates; error bars represent the SD. Calculated numerical values are related to the sample fresh weight (µg g^{-1} FW). n.d, not detectable. (B) Proposed model of JAZ10 stabilization and MYC3 inhibition by the fungal effector Tue1. Left panel: In the presence of a pathogen, JAZ10 is targeted for degradation via the JA-dependent pathway, relieving the repression of MYC3. MYC3, together with the co-activator MED25, promotes the expression of JA-responsive genes. Right panel: When Tue1 is present, it binds to the Jas domain of JAZ10, stabilizing the repressor and preventing its degradation. Stabilized JAZ10 sequesters MYC3 via its CMID domain, thereby blocking the transcriptional activation of JA-responsive genes and reducing JA signalling output.

interactions. Our analysis might serve as a starting point to investigate how these Tin2-fold effectors diversified and whether some share similar functions despite their broad distribution across different biological systems.

Tue1 binds to JAZ10 and represses plant jasmonate levels

Our study demonstrates that Tue1 specifically binds to JAZ10, a key repressor of JA-responsive genes, and interferes with plant hormone concentrations. JA signalling plays a pivotal role in plant defence against fungal pathogens (Antico *et al.*, 2012). Upon fungal detection, plants activate the JA pathway, resulting in the induction of defence-related genes and the production of protective secondary metabolites. The perception of JA is mediated by the receptor COI1, an E3 ligase that targets JAZ repressors for degradation (Li *et al.*, 2021; Zhu, 2023).

Owing to their central role in plant defence, JAZ proteins are targeted by different pathogens through a variety of mechanisms. For instance, the bacterial phytotoxin coronatine mimics JA-Ile, thereby activating COI1-dependent proteasomal degradation of JAZ repressors and reopening stomata to promote bacterial entry (Melotto *et al.*, 2008; Panchal and Melotto, 2017). The two bacterial effectors HopZ1 and HopX1 from *Pseudomonas syringae* pv. *tomato* DC3000 directly target JAZ proteins such as JAZ2, which plays a role in stomatal

Downloaded from https://academic.oup.com/jxb/article/76/22/7051/8245658 by Deutsches Elektronen Synchrotron DESY user on 15 January 2026

dynamics during bacterial infection (Gimenez-Ibanez *et al.*, 2017). HopZ1 acetylates the JAZ repressors, leading to their degradation (Jiang *et al.*, 2013); HopX1 is a cysteine protease that directly degrades the JAZ repressor independently of COI1 and the proteasome (Gimenez-Ibanez *et al.*, 2014). Notably, COI1 and HopZ1 interact with the Jas domain, the binding site for MYC transcription factors (Takaoka *et al.*, 2022), whereas HopX1 binds to the ZIM domain, demonstrating that different JAZ domains can be targeted by effectors. Importantly, these bacterial effectors are active enzymes that modify their targets through acetylation or direct degradation (Jiang *et al.*, 2013; Gimenez-Ibanez *et al.*, 2014).

In contrast to bacterial effectors, fungal effectors that target JA signalling are less well characterized and generally lack catalytic activity. One example is MiSSP7 from the ectomycorrhizal fungus *Laccaria bicolor*, which interacts with and stabilizes poplar JAZ6, thereby suppressing a subset of JA-responsive genes (Plett *et al.*, 2014). Mechanistically, MiSSP7 reinforces the interaction between JAZ6 and MYC2.1, preventing JAZ6 oligomerization and selectively modulating JA responses (Daguerre *et al.*, 2020). Interestingly, only a limited fraction of JA-regulated genes is affected by MiSSP7, likely due to redundancy among JAZ proteins (Pauwels and Goossens, 2011). When comparing gene expression changes from *L. bicolor* colonization with our transcriptomic data, we observed minimal overlap, indicating that Tue1 acts through a distinct mechanism (Supplementary Table S8).

In *A. thaliana*, overexpression of Tue1 causes JA concentrations to drop below the detection limit of the assay used (Fig. 6A). MST experiments revealed that Tue1 binds to the Jas domain of JAZ10 (Supplementary Fig. S6B), a region also involved in interactions with transcriptional activators such as MYC3. This interaction likely leads to JAZ10 stabilization and prevents MYC3 binding. Importantly, the CMID domain of JAZ10 remains available to bind MYC3, potentially allowing it to be sequestered and thereby blocking the activation of JA-responsive genes. Our data thus support a model in which Tue1 stabilizes JAZ10 by binding to its Jas domain, indirectly reinforcing the repression of JA signalling by facilitating MYC3 sequestration (Fig. 6B).

This suppression of JA responses may help *T. thlaspeos* maintain a prolonged biotrophic phase and symptomless colonization, as low JA levels are associated with increased fungal accommodation, as observed in *Azoarcus olearius* colonization of rice (Chen *et al.*, 2019). This strategy may also reduce direct fungal–plant cell interactions, as seen in *U. maydis*. However, since multiple effectors are expressed during the biotrophic phase, the specific contribution of Tue1 to transcriptomic changes is difficult to disentangle. Further research is needed to fully understand the functional relevance of the Tue1–JAZ10 interaction and to elucidate the precise molecular mechanism of action of Tue1.

In conclusion, our findings provide the first mechanistic insights into an effector from the smut fungus *T. thlaspeos*, showing that it supports plant infection by directly binding to JAZ10 in both *A. thaliana* and *A. hirsuta*. Our structural analysis furthermore suggests the expansion of Tin2-fold effectors to even distantly related smut fungi such as *T. thlaspeos*, providing evidence for evolutionary conservation of this family.

Supplementary data

The following supplementary data are available at *JXB* online.

Fig. S1. Structural model of *A. thaliana* importin-α in complex with the Tue1-NLS.
Fig. S2. Size-exclusion chromatogram of Tue1.
Fig. S3. Multiple sequence alignment of Tue1, Tue16, and THTG_04670.
Fig. S4. Auto-activity test of Tue1 in yeast.
Fig. S5. Sequence alignment of *A. hirsuta* and *A. thaliana* homologs of JAZ10.
Fig. S6. Microscale thermophoresis dose–response curves of Tue1, Tue16, and MYC3 with JAZ10.
Fig. S7. Western blots of protein expression for BiFC experiments.
Table S1. Plasmids used in this study.
Table S2. Oligonucleotides used in this study.
Table S3. Strains used in this study.
Table S4. Plant lines used in this study.
Table S5. Crystallographic data collection and refinement statistics of Tue1.
Table S6. Selected candidates from the Y2H screen.
Table S7. Affinities from microscale thermophoresis.
Table S8. Comparison of JA-inducible genes repressed by MiSSP7 with the transcriptomic analysis of infected *A. hirsuta*.
Dataset S1. Structural clustering data.
Dataset S2. Microscale thermophoresis data.
Dataset S3. Y2H analysis with a stress-induced cDNA library of *A. thaliana* leaves.

Acknowledgements

We thank Michael Feldbrügge and Kerstin Schipper for critical reading and fruitful discussions on the manuscript. We are grateful to Maeli Melotto for providing the cDNA library and support.

Author contributions

VG, FA: conceptualization; FA: formal analysis; SuG, GMR, StG, MH, NH: investigation; JZ, SHJS: resources; MH, NH: data curation; SuG, GMR, FA, VG: writing—original draft; FA, VG: writing—review & editing; SuG, GMR, FA: visualization; FA, VG: supervision; SHJS, FA, VG: funding acquisition.

Conflict of interest

The authors declare no conflict of interest.

Funding

The Center for Structural Studies is funded by the Deutsche Forschungsgemeinschaft (DFG, German Research Foundation; grant numbers 417919780, INST 208/740-1 FUGG, and INST 208/868-1 FUGG to SHJS). This work was supported by the Deutsche Forschungsgemeinschaft under Germany's Excellence Strategy—EXC 2048/1—Project ID 390686111 (to FA, VG and JZ), CRC1535—

Downloaded from https://academic.oup.com/jxb/article/76/22/7051/8245658 by Deutsches Elektronen Synchrotron DESY user on 15 January 2026

Project ID 458090666 (to FA and SHJS), and GRK2466—Project ID 391465903 (to VG and GMR). SG was supported by a doctoral fellowship of the Schlumberger Foundation Faculty for the Future program. The funders did not have a role in experimental planning, data analysis, or manuscript preparation.

Data availability

The data underlying this article are available in the article and in its online supplementary material. Crystallographic data of Tue1 are available in the Protein Data Bank (https://www.rcsb.org) at https://doi.org/10.2210/pdb9FPM/pdb.

References

Adams PD, Afonine PV, Bunkóczi G, *et al.* 2010. PHENIX: a comprehensive Python-based system for macromolecular structure solution. Acta Crystallographica: Section D, Biological Crystallography **66**, 213–221.

Antico CJ, Colon C, Banks T, Ramonell KM. 2012. Insights into the role of jasmonic acid-mediated defenses against necrotrophic and biotrophic fungal pathogens. Frontiers in Biology **7**, 48–56.

Brefort T, Tanaka S, Neidig N, Doehlemann G, Vincon V, Kahmann R. 2014. Characterization of the largest effector gene cluster of *Ustilago maydis*. PLoS Pathogens **10**, e1003866.

Chen X, Marszałkowska M, Reinhold-Hurek B. 2019. Jasmonic acid, not salicyclic acid restricts endophytic root colonization of rice. Frontiers in Plant Science **10**, 1758.

Courville KJ, Frantzeskakis L, Gul S, *et al.* 2019. Smut infection of perennial hosts: the genome and the transcriptome of the Brassicaceae smut fungus *Thecaphora thlaspeos* reveal functionally conserved and novel effectors. New Phytologist **222**, 1474–1492.

Cutler SR, Ehrhardt DW, Griffitts JS, Somerville CR. 2000. Random GFP::cDNA fusions enable visualization of subcellular structures in cells of *Arabidopsis* at a high frequency. Proceedings of the National Academy of Sciences, USA **97**, 3718–3723.

Daguerre Y, Basso V, Hartmann-Wittulski S, Schellenberger R, Meyer L, Bailly J, Kohler A, Plett JM, Martin F, Veneault-Fourrey C. 2020. The mutualism effector MiSSP7 of *Laccaria bicolor* alters the interactions between the poplar JAZ6 protein and its associated proteins. Scientific Reports **10**, 20362.

Deak M, Kiss GB, Koncz C, Dudits D. 1986. Transformation of *Medicago* by *Agrobacterium* mediated gene transfer. Plant Cell Reports **5**, 97–100.

Derbyshire MC, Raffaele S. 2023. Surface frustration re-patterning underlies the structural landscape and evolvability of fungal orphan candidate effectors. Nature Communications **14**, 5244.

EFSA Panel on Plant Health (PLH), Bragard C, Dehnen-Schmutz K, *et al.* 2018. Pest categorisation of *Thecaphora solani*. Food Safety Journal **16**, e05445.

Emsley P, Cowtan K. 2004. Coot: model-building tools for molecular graphics. Acta Crystallographica: Section D, Biological Crystallography **60**, 2126–2132.

Fernández-Calvo P, Chini A, Fernández-Barbero G, *et al.* 2011. The *Arabidopsis* bHLH transcription factors MYC3 and MYC4 are targets of JAZ repressors and act additively with MYC2 in the activation of jasmonate responses. The Plant Cell **23**, 701–715.

Fisher MC, Henk DA, Briggs CJ, Brownstein JS, Madoff LC, McCraw SL, Gurr SJ. 2012. Emerging fungal threats to animal, plant and ecosystem health. Nature **484**, 186–194.

Frantzeskakis L, Courville KJ, Plucker L, Kellner R, Kruse J, Brachmann A, Feldbrugge M, Gohre V. 2017. The plant-dependent life cycle of *Thecaphora thlaspeos*: a smut fungus adapted to Brassicaceae. Molecular Plant-Microbe Interactions **30**, 271–282.

Gimenez-Ibanez S, Boter M, Fernández-Barbero G, Chini A, Rathjen JP, Solano R. 2014. The bacterial effector HopX1 targets JAZ transcriptional repressors to activate jasmonate signaling and promote infection in *Arabidopsis*. PLoS Biology **12**, e1001792.

Gimenez-Ibanez S, Boter M, Ortigosa A, García-Casado G, Chini A, Lewsey MG, Ecker JR, Ntoukakis V, Solano R. 2017. JAZ2 controls stomata dynamics during bacterial invasion. New Phytologist **213**, 1378–1392.

Hartmann M, Zeier T, Bernsdorff F, *et al.* 2018. Flavin monooxygenase-generated N-hydroxypipecolic acid is a critical element of plant systemic immunity. Cell **173**, 456–469.e16.

Hemetsberger C, Mueller AN, Matei A, *et al.* 2015. The fungal core effector Pep1 is conserved across smuts of dicots and monocots. New Phytologist **206**, 1116–1126.

Hoeksema JD, Bever JD, Chakraborty S, *et al.* 2018. Evolutionary history of plant hosts and fungal symbionts predicts the strength of mycorrhizal mutualism. Communications Biology **1**, 116.

Hooper CM, Castleden IR, Tanz SK, Aryamanesh N, Millar AH. 2017. SUBA4: the interactive data analysis centre for Arabidopsis subcellular protein locations. Nucleic Acids Research **45**, D1064–D1074.

Huang L, Ökmen B, Stolze SC, Kastl M, Khan M, Hilbig D, Nakagami H, Djamei A, Doehlemann G. 2024. The fungal pathogen *Ustilago maydis* targets the maize corepressor RELK2 to modulate host transcription for tumorigenesis. New Phytologist **241**, 1747–1762.

Jiang S, Yao J, Ma K-W, Zhou H, Song J, He SY, Ma W. 2013. Bacterial effector activates jasmonate signaling by directly targeting JAZ transcriptional repressors. PLoS Pathogens **9**, e1003715.

Jumper J, Evans R, Pritzel A, *et al.* 2021. Highly accurate protein structure prediction with AlphaFold. Nature **596**, 583–589.

Kabsch W. 2010. XDS. Acta Crystallographica: Section D, Biological Crystallography **66**, 125–132.

Kämper J, Kahmann R, Bölker M, *et al.* 2006. Insights from the genome of the biotrophic fungal plant pathogen *Ustilago maydis*. Nature **444**, 97–101.

Khan M, Uhse S, Bindics J, Kogelmann B, Nagarajan N, Tabassum R, Ingole KD, Djamei A. 2024. Tip of the iceberg? Three novel TOPLESS-interacting effectors of the gall-inducing fungus *Ustilago maydis*. New Phytologist **244**, 949–961.

Koncz C, Schell J. 1986. The promoter of T_L-DNA gene *5* controls the tissue-specific expression of chimeric genes carried by a novel type of *Agrobacterium* binary vector. Molecular and General Genetics **204**, 383–396.

Kosugi S, Hasebe M, Tomita M, Yanagawa H. 2009. Systematic identification of cell cycle-dependent yeast nucleocytoplasmic shuttling proteins by prediction of composite motifs. Proceedings of the National Academy of Sciences, USA **106**, 10171–10176.

Krishna R, Wang J, Ahern W, *et al.* 2024. Generalized biomolecular modeling and design with RoseTTAFold All-Atom. Science **384**, eadl2528.

Lampropoulos A, Sutikovic Z, Wenzl C, Maegele I, Lohmann JU, Forner J. 2013. GreenGate - a novel, versatile, and efficient cloning system for plant transgenesis. PLoS One **8**, e83043.

Lanver D, Tollot M, Schweizer G, *et al.* 2017. *Ustilago maydis* effectors and their impact on virulence. Nature Reviews: Microbiology **15**, 409–421.

Laurie JD, Ali S, Linning R, *et al.* 2012. Genome comparison of barley and maize smut fungi reveals targeted loss of RNA silencing components and species-specific presence of transposable elements. The Plant Cell **24**, 1733–1745.

Lefebvre F, Joly DL, Labbe C, Teichmann B, Linning R, Belzile F, Bakkeren G, Belanger RR. 2013. The transition from a phytopathogenic smut ancestor to an anamorphic biocontrol agent deciphered by comparative whole-genome analysis. The Plant Cell **25**, 1946–1959.

Li M, Yu G, Cao C, Liu P. 2021. Metabolism, signaling, and transport of jasmonates. Plant Communications **2**, 100231.

Lo Presti L, Lanver D, Schweizer G, Tanaka S, Liang L, Tollot M, Zuccaro A, Reissmann S, Kahmann R. 2015. Fungal effectors and plant susceptibility. Annual Review of Plant Biology **66**, 513–545.

Downloaded from https://academic.oup.com/jxb/article/76/22/7051/8245658 by Deutsches Elektronen Synchrotron DESY user on 15 January 2026

Mansoor S, Baek M, Juergens D, Watson JL, Baker D. 2023. Zero-shot mutation effect prediction on protein stability and function using RoseTTAFold. Protein Science **32**, e4780.

Matiolli CC, Melotto M. 2018. A comprehensive *Arabidopsis* yeast two-hybrid library for protein-protein interaction studies: a resource to the plant research community. Molecular Plant-Microbe Interactions **31**, 899–902.

Melotto M, Underwood W, He SY. 2008. Role of stomata in plant innate immunity and foliar bacterial diseases. Annual Reviews in Phytopathology **46**, 101–122.

Nguyen Ba AN, Pogoutse A, Provart N, Moses AM. 2009. NLStradamus: a simple Hidden Markov Model for nuclear localization signal prediction. BMC Bioinformatics **10**, 202.

Panchal S, Melotto M. 2017. Stomate-based defense and environmental cues. Plant Signaling & Behavior **12**, e1362517.

Paredes JA, Cazón LI, Conforto EC, Rago A. 2024. Peanut smut in Argentina: an analysis of the disease, advances, and challenges. Plant Disease **108**, 2593–2606.

Pauwels L, Goossens A. 2011. The JAZ proteins: a crucial interface in the jasmonate signaling cascade. The Plant Cell **23**, 3089–3100.

Pettersen EF, Goddard TD, Huang CC, Meng EC, Couch GS, Croll TI, Morris JH, Ferrin TE. 2021. UCSF ChimeraX: structure visualization for researchers, educators, and developers. Protein Science **30**, 70–82.

Plett JM, Daguerre Y, Wittulsky S, ***et al.*** 2014. Effector MiSSP7 of the mutualistic fungus *Laccaria bicolor* stabilizes the *Populus* JAZ6 protein and represses jasmonic acid (JA) responsive genes. Proceedings of the National Academy of Sciences, USA **111**, 8299–8304.

Plücker L, Bosch K, Geißl L, Hoffmann P, Göhre V. 2021. Genetic manipulation of the Brassicaceae smut fungus *Thecaphora thlaspeos*. Journal of Fungi **7**, 38.

Puginier C, Keller J, Delaux PM. 2022. Plant-microbe interactions that have impacted plant terrestrializations. Plant Physiology **190**, 72–84.

Rutter BD, Innes RW. 2017. Extracellular vesicles isolated from the leaf apoplast carry stress-response proteins. Plant Physiology **173**, 728–741.

Schirawski J, Mannhaupt G, Münch K, ***et al.*** 2010. Pathogenicity determinants in smut fungi revealed by genome comparison. Science **330**, 1546–1548.

Schuster M, Schweizer G, Kahmann R. 2018. Comparative analyses of secreted proteins in plant pathogenic smut fungi and related basidiomycetes. Fungal Genetics and Biology **112**, 21–30.

Seong K, Krasileva KV. 2023. Prediction of effector protein structures from fungal phytopathogens enables evolutionary analyses. Nature Microbiology **8**, 174–187.

Sharma R, Mishra B, Runge F, Thines M. 2014. Gene loss rather than gene gain is associated with a host jump from monocots to dicots in the smut fungus *Melanopsichium pennsylvanicum*. Genome Biology and Evolution **6**, 2034–2049.

Sperschneider J, Catanzariti AM, DeBoer K, Petre B, Gardiner DM, Singh KB, Dodds PN, Taylor JM. 2017. LOCALIZER: subcellular localization prediction of both plant and effector proteins in the plant cell. Scientific Reports **7**, 44598.

Takaoka Y, Suzuki K, Nozawa A, Takahashi H, Sawasaki T, Ueda M. 2022. Protein–protein interactions between jasmonate-related master regulator MYC and transcriptional mediator MED25 depend on a short binding domain. Journal of Biological Chemistry **298**, 101504.

Tanaka S, Brefort T, Neidig N, Djamei A, Kahnt J, Vermerris W, Koenig S, Feussner K, Feussner I, Kahmann R. 2014. A secreted *Ustilago maydis* effector promotes virulence by targeting anthocyanin biosynthesis in maize. eLife **3**, e01355.

Tanaka S, Han X, Kahmann R. 2015. Microbial effectors target multiple steps in the salicylic acid production and signaling pathway. Frontiers in Plant Science **6**, 349.

Tanaka S, Schweizer G, Rössel N, Fukada F, Thines M, Kahmann R. 2019. Neofunctionalization of the secreted Tin2 effector in the fungal pathogen *Ustilago maydis*. Nature Microbiology **4**, 251–257.

Teufel F, Almagro Armenteros JJ, Johansen AR, Gíslason MH, Pihl SI, Tsirigos KD, Winther O, Brunak S, von Heijne G, Nielsen H. 2022. Signalp 6.0 predicts all five types of signal peptides using protein language models. Nature Biotechnology **40**, 1023–1025.

van Kempen M, Kim SS, Tumescheit C, Mirdita M, Lee J, Gilchrist CLM, Söding J, Steinegger M. 2023. Fast and accurate protein structure search with Foldseek. Nature Biotechnology **42**, 243–246.

Vánky K. 2008. Smut fungi (*Basidiomycota* P.P., *Ascomycota* P.P.) of the world. Novelties, selected examples, trends. Acta Microbiologica et Immunologica Hungarica **55**, 91–109.

Yildiz I, Gross M, Moser D, Petzsch P, Köhrer K, Zeier J. 2023. N-hydroxypipecolic acid induces systemic acquired resistance and transcriptional reprogramming via TGA transcription factors. Plant, Cell & Environment **46**, 1900–1920.

Zhang Y, Skolnick J. 2005. TM-align: a protein structure alignment algorithm based on the TM-score. Nucleic Acids Research **33**, 2302–2309.

Zhu Z. 2023. Jasmonate: the Swiss army knife in the plant's pocket. Journal of Experimental Botany **74**, 1159–1161.

Zuo W, Ökmen B, Depotter JRL, Ebert MK, Redkar A, Misas Villamil J, Doehlemann G. 2019. Molecular interactions between smut fungi and their host plants. Annual Review of Phytopathology **57**, 411–430.

Zuo W, Depotter JRL, Stolze SC, Nakagami H, Doehlemann G. 2023. A transcriptional activator effector of *Ustilago maydis* regulates hyperplasia in maize during pathogen-induced tumor formation. Nature Communications **14**, 6722.

Zweng S, Mendoza-Rojas G, Lepak A, Altegoer F. 2025. Simplifying recombinant protein production: combining Golden Gate cloning with a standardized protein purification scheme. Methods in Molecular Biology **2850**, 229–249.

Downloaded from https://academic.oup.com/jxb/article/76/22/7051/8245658 by Deutsches Elektronen Synchrotron DESY user on 15 January 2026